SUPPORTING INFORMATION

Understanding the Nature of the Passivation Layer Enabling Calcium Plating

Juan Forero-Saboya,[a] Carine Davoisne,[b,f,g] Rémi Dedryvère,[c,f,g] Ibraheem Yousef,[d] Pieremanuele Canepa,[e] Alexandre Ponrouch[a,f]

[a]Institut de Ciència de Materials de Barcelona (ICMAB-CSIC), Campus UAB, 08193 Bellaterra, Catalonia, Spain.
[b]Laboratoire de Réactivité et Chimie des Solides, Université de Picardie Jules Verne, CNRS UMR7314, 33 rue Saint Leu, 80039 Amiens,France
[c]UPPA/CNRS/Université Pau & Pays Adour, 64000 Pau, France
[d]MIRRAS Beamline, ALBA Synchrotron Light Source, Carrer de la Llum, 2-26, 08290 Cerdanyola del Vallès, Barcelona, Spain
[e]Department of Materials Science and Engineering, The National University of Singapore, 117576, Singapore
[f]ALISTORE – European Research Institute, CNRS FR 3104, Hub de l'Energie, 15 Rue Baudelocque, 80039 Amiens, France
[g]Réseau sur le Stockage Electrochimique de l'Energie (RS2E) - FR CNRS 3459, 80039 Amiens Cedex, France

CONTENTS

1. EXPERIMENTAL DETAILS

Materials

The electrolytes investigated are $Ca(TFSI)_2$ (calcium bis[trifluoromethanesulphonimide], 99,9% Solvionic) or $Ca(BF_4)_2$ (hydrate, from Alfa Aesar) dissolved in a 50/50 wt% mixture of propylene carbonate (PC, from Aldrich, anhydrous, 99.7%) and ethylene carbonate (EC, from Aldrich, anhydrous, 99.0%). To reduce the water contamination, the solvent mixtures were dried over molecular sieves (~3Å, from Alfa Aesar) for at least two days before the preparation of the electrolytes, whereas all salts were vacuum-dried at moderate temperatures (100 °C) before their use.

Sample preparation, characterization and chemical analysis of the electrode surfaces

All deposits were prepared following the experimental conditions reported previously for calcium plating.[1] Namely, the deposits were formed upon constant polarization (–1.4 V vs. Ca) for 48 hours at 100 °C and using calcium-metal (98%, from Alfa Aesar) as both the reference and the counter electrodes. Two different electrolytes salts were used in the study, i.e. $Ca(TFSI)_2$ and $Ca(BF4)_2$. In both cases the salt concentration was fixed to 0.45 M and the salt was dissolved in a EC:PC mixture (50:50 wt%). The cells were assembled and disassembled inside an argon filled glovebox with O_2 and H_2O concentrations below 5 ppm.

For the characterization with transmission electron microscopy (TEM), ~40 mg of nickel powder (99.9 %, APS 3-7 micron, from Alfa Aesar) was used as the working electrode (WE) without additional binders or additives. The use of metallic powder was required for TEM study as only micrometric particles allow for the investigation of the thickness and morphology of passivation layer in transmission mode. In this specific case, Ni powder provided the best compromise between particle size and inertness against alloying with Ca. The integrity of the electrode and the electrical contact between the particles were sustained only by the pressure of the cell. After polarization of the WE at –1.4 V vs. Ca, the powder was rinsed several times with dimethyl carbonate (DMC), dispersed and placed over copper TEM grids with plain carbon film.

The transfer between the argon filled glove box and the TEM was performed without air exposure according the procedure described by Dupont et *al*.[2] The microstructural and chemical characterizations of the electrodes were performed using a TECNAI F20-S-Twin operating at 200kV and equipped with an electron energy loss Spectrometer (EELS) GIF Tridiem in post column. The acquisitions of the energy-loss near-edge structures (ELNES) were performed in diffraction or scanning transmission electron microscopy (STEM) modes. The reported measurements were performed using an energy resolution of 1–1.2 eV and determined by measuring the full-width at half maximum of the zero-loss peak. The following conditions were used to acquire the EELS spectra: a dispersion of 0.2 eV/ch, a convergence angle of 5.8 mrad and a collection angle of 21.7 mrad, respectively. For the core loss of the B and the Ca K-edges: the background was subtracted considering a power-law function.[3] The multiple scatterings were removed using the Fourier-ratio method

and energy correction was performed with respect to the C K-edge of amorphous carbon, whose main feature is at ~285 eV. To limit the irradiation effect and give reliable results, the TEM/EELS investigations were done in low dose mode and using specific tunings determined after a prior irradiation study on the samples. The tuning and the analyses were also performed on different areas to avoid unnecessary irradiation on the area of interest.

In the case of Fourier-transform infrared spectroscopy (FTIR) and X-ray photoelectron spectroscopy (XPS), a disk of Ca metal was used as WE. After polarization of the disks in the respective electrolytes, FTIR measurements of the surface films were acquired on a Vertex 70 Spectrometer using a praying mantis diffuse reflectance accessory (HARRICK) to prevent any air exposure. To improve the spatial resolution of the FTIR instrument, a Vector 70 spectrometer was coupled to a Hyperion 3000 microscope to perform Synchrotron-based FTIR microspectroscopy measurements at the MIRAS beamline of the ALBA synchrotron light source (Barcelona, Spain). The microscope is equipped with a liquid N_2 cooled HgCdTe 50 µm MCT detector and uses a 36X Schwarzschild objective (NA=0.52). The spectra were obtained in trans-reflection mode, using a masking aperture size of 50 µm x 50 µm. Raster scanning maps were collected in the mid-IR range (4000-700 cm^{-1}) at a spectral resolution of 4 cm^{-1} with 256 co-added scans per spectrum.

X-ray Photoelectron Spectroscopy (XPS) was carried out with a Thermo Scientific Escalab 250 Xi spectrometer using a focused monochromatic radiation at two different photon energies: Al Kα (hν = 1486.6 eV) and Ag Lα (hν = 2984.2 eV). The analyzed area of the samples was an ellipse with dimension of 450 × 900 μm^2. Peaks were recorded with a constant pass energy of ~20 eV. The binding energy scale was calibrated from the hydrocarbon contamination using the C *1s* peak at 285.0 eV. For all analyses, caution was exercised to prevent the samples surface from any contact with air and moisture. All samples were handled or stored in controlled dry argon atmosphere and the XPS transfer chamber was directly connected to the argon glovebox. The electrodes were washed by 3×1 min immersion in pure anhydrous DMC baths to get rid of the electrolyte. DMC was then evaporated by leaving the electrode under vacuum (inside the glovebox antechamber).

Electrochemical measurements

Cyclic voltammetry (CV) experiments were performed in a three-electrode Swagelok cells setup, using stainless-steel as WE, calcium disks (Alfa Aesar, 99.5%) as counter and reference electrodes, respectively. A Whatman glass microfiber separator was used. All electrochemical tests were performed using a Bio-Logic VSP300 potentiostat. All cells were assembled in an Ar-filled glovebox (O_2 and H_2O below 1 ppm) and sealed before their transfer to an oven at 100 °C.

To pre-passivate the surface of the stainless-steel electrodes, the protocol consisted in cycling the clean stainless-steel electrodes for 10 cycles in a solution of 0.45 M $Ca(BF_4)_2$ at 0.1 mV/s between 0.1 and -

1.4 V vs. Ca at 100 °C using three-electrode cells with calcium disks as reference and counter electrodes. After the passivation, the cells were disassembled, the electrodes were washed thoroughly using dimethyl carbonate and dried under vacuum before the cell were reassembled using the same three electrodes.

Computational Details

To model the migration of Ca^{2+} and Mg^{2+} ions in selected host structures, we use the nudged elastic band (NEB)[4,5] method together with density functional theory (DFT),[6,7] where the exchange and correlation functional is parametrized by the Perdew–Burke–Ernzerhof Generalized-Gradient Approximation (GGA)[8] as implemented in VASP.[9] To properly include Van der Waals forces the *a posteriori* correction proposed by Grimme was used.[10] The total energy was sampled using a *k*-point mesh with density of 1000/(number of atoms per unit cell). The Projector augmented-wave theory together with a plane-wave cutoff of 520 eV were employed to describe the core and valence electrons wave functions, respectivelly.[11] The convergence threshold of the total energy was set to $1x10^{-6}$ eV, whereas the forces during the geometry relaxations of the end-point images were converged to $1x10^{-2}$ eV/Å.

In the NEB calculations, eight images were lineally interpolated between the end points used to prepare the initial migration energy paths. In order to avoid spurious interactions between images during the relaxation of the NEBs, supercells of appropriate sizes were used to ensure a minimum inter-image distance of 8 Å. In the NEB calculations the forces on the elastic band were converge to 0.05 eV/ Å. The calculations were performed in the dilute vacancy limit, which in the simplest scenario required one Ca^{2+} (Mg^{2+}) ion to be removed per unit cell. Given that the compounds investigated do not contain transition metals, upon Ca^{2+} (Mg^{2+}) removal the neutrality of the system is maintained via a jellium counter-charge and following the protocol proposed by Chen *et al.*[12]

Similar to what have been calculated previously for cathode materials,[12,13] maximum tolerable migration barrier E_m were estimated the migration ion needs to overcome to allow ion percolation. Diffusion length μ scales was considered as $\mu = \sqrt{Dt}$ (with D the diffusivity and t time), assuming a random walk for ion diffusion in the particle, and accepting that the local ion migration follows an Arrhenius-like relationship $D = \nu a^2 \exp(-E_m/k_B T)$. In the Arrhenius expression, we set the jump frequency to $\nu \approx 10^{12}$ s^{-1} and the atomic jump distance $a \approx 3$ Å, which is in the range of typical lattice parameters. We note that because of the exponential nature of the Arrhenius equation, change in the barrier of ±50 meV –the typical accuracy of NEB calculations– propagates as ±1 order of magnitude in diffusivity.

2. SUPPLEMENTARY TABLES

Table S1: Binding energy (eV) and atomic percentage (%) of the components observed in XPS spectra reported in figure 2 after polarizing Ca disks at –1.4 V vs. a Ca reference electrode for 48 hours in two different electrolytes: 0.45 M $Ca(TFSI)_2$ or $Ca(BF_4)_2$ in a EC:PC mixture (50:50 wt%).

Peak	**$Ca(TFSI)_2$**		**$Ca(BF_4)_2$**		**Chemical attribution**
	BE (eV)	%	BE (eV)	%	
C 1s	285.0	7.2	284.8	20.9	C-C, C-H
	286.7	5.6	286.4	11.4	C-O
	---	---	287.7	2.5	C=O
	288.4	2.7	---	---	COO
	290.0	6.7	290.6	1.6	$CaCO_3$
	293.1	1.1	---	---	$Ca(TFSI)_2$
O 1s	531.7	47.2	531.8	32.9	unresolved oxygen species
Ca $2p_{3/2}$	347.5	24.2	---	---	$CaCO_3$ + CaO (+ CaF_2 + $Ca(TFSI)_2$)
	---	---	348.0	6.9	CaF_2 + $CaCO_3$
F 1s	684.7	1.6	684.6	10.2	CaF_2
	688.6	2.2	---	---	$Ca(TFSI)_2$
N 1s	399.2	0.5	---	---	$Ca(TFSI)_2$
S $2p_{3/2}$	169.0	1.0	---	---	$Ca(TFSI)_2$
B 1s	---	---	191.9	13.6	borate environment

Table S2: Binding energy (eV) and atomic percentage (%) of the components observed in XPS spectra reported in Figure S4 after polarizing a Mg disk at –1.4 V vs. a Mg reference electrode for 48 hours in 0.45M $Mg(TFSI)_2$ electrolyte in a EC:PC mixture (50:50 wt%).

Peak	**$Mg(TFSI)_2$**		**Chemical attribution**
	BE (eV)	%	
C 1s	285.0	7.5	C-C, C-H
	286.7	3.6	C-O
	289.4	2.9	O=C-O
	290.3	3.5	$MgCO_3$
	293.1	1.0	$Mg(TFSI)_2$
O 1s	532.5	38.3	unresolved oxygen species
Mg 2p	49.4	7.7	Mg metal
	50.9	26.7	all other Mg species
F 1s	685.5	3.8	MgF_2
	688.8	3.9	$Mg(TFSI)_2$
N 1s	---	---	(not detected due to Mg Auger tail)
S $2p_{3/2}$	169.4	1.1	$Mg(TFSI)_2$

3. SUPPLEMENTARY FIGURES

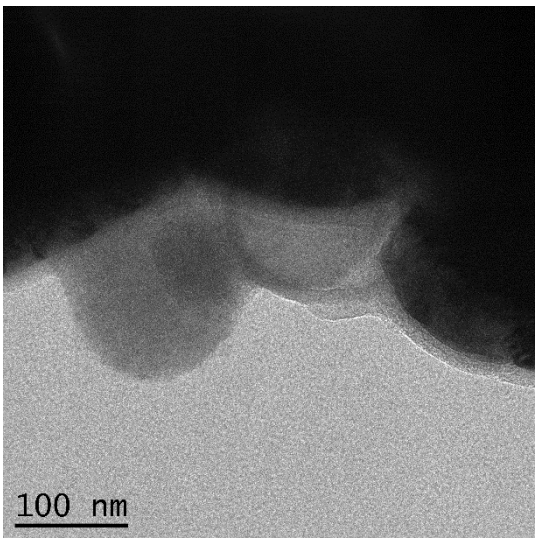

Figure S1. Bright Field TEM images of Ni particles after formation of a surface layer in $Ca(TFSI)_2$ based electrolytes. While most of the passivation layer covering the Ni particle is thin (less than 20 nm) and smooth, few protruding passivation areas can be observed.

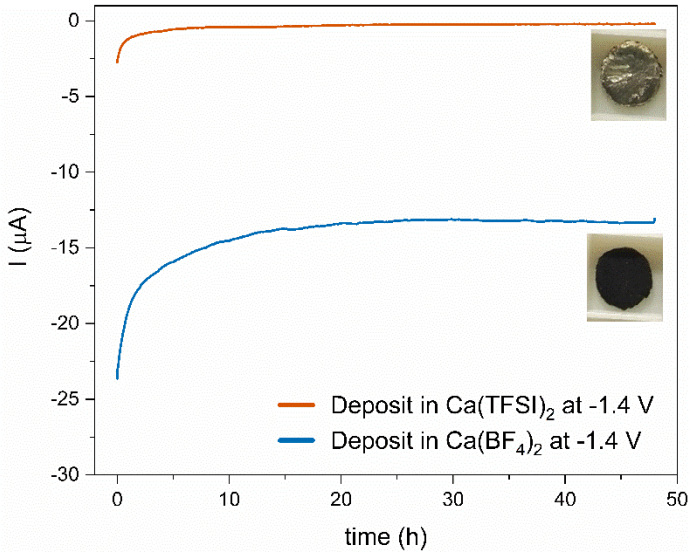

Figure S2. Reductive current recorded during polarization of a Ca disk at -1.4 V vs. a Ca metal reference in BF_4^-- and TFSI- based electrolytes. Inset: pictures of the Ca disks employed as working electrodes at the end of the polarization treatment in each electrolyte.

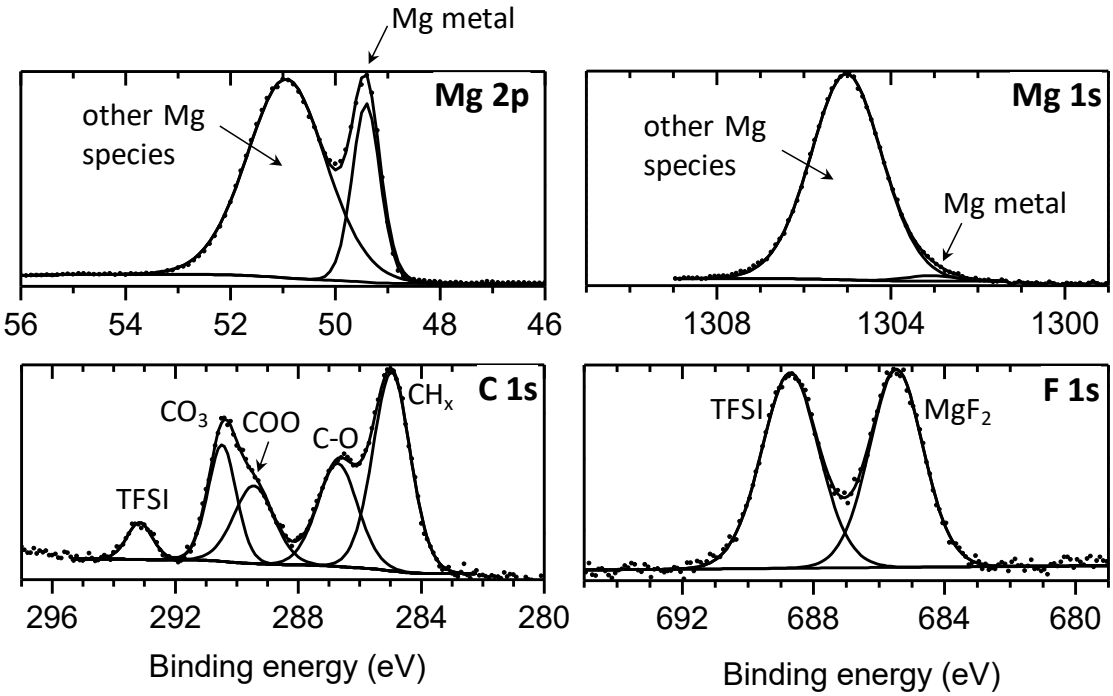

Figure S3. XPS spectra of the passivation film formed on a Mg metal anode during negative polarization in an electrolyte composed of 0.45 M $Mg(TFSI)_2$ in EC:PC. For Mg 2p the metallic Mg signal is easily detected. For Mg 1s the probe depth is much lower and the metallic Mg signal is hidden by outermost surface species.

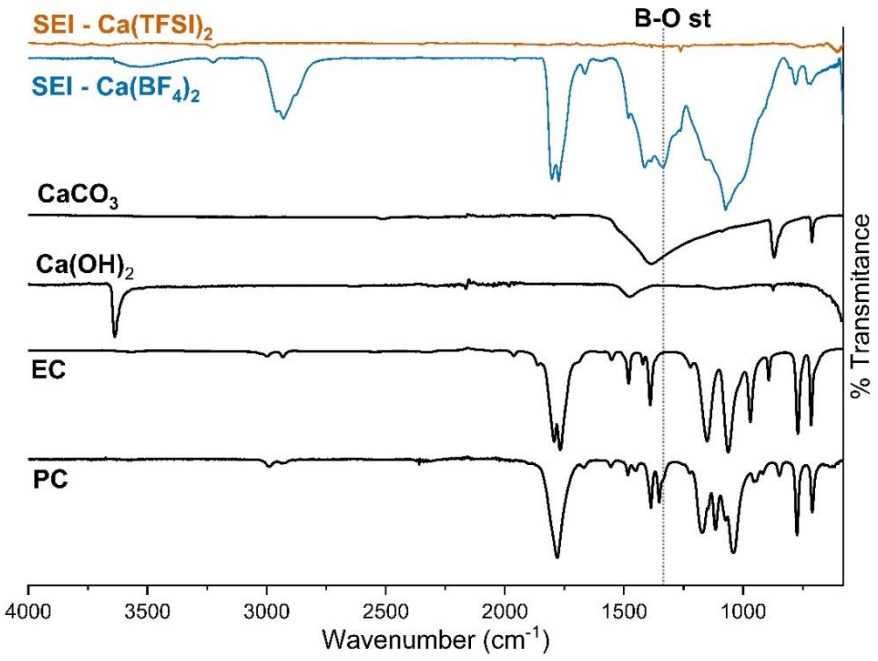

Figure S4. Full IR spectra of the passivation layer deposited on a calcium disk upon polarization for 48h in $Ca(BF_4)_2$ and $Ca(TFSI)_2$ electrolytes.

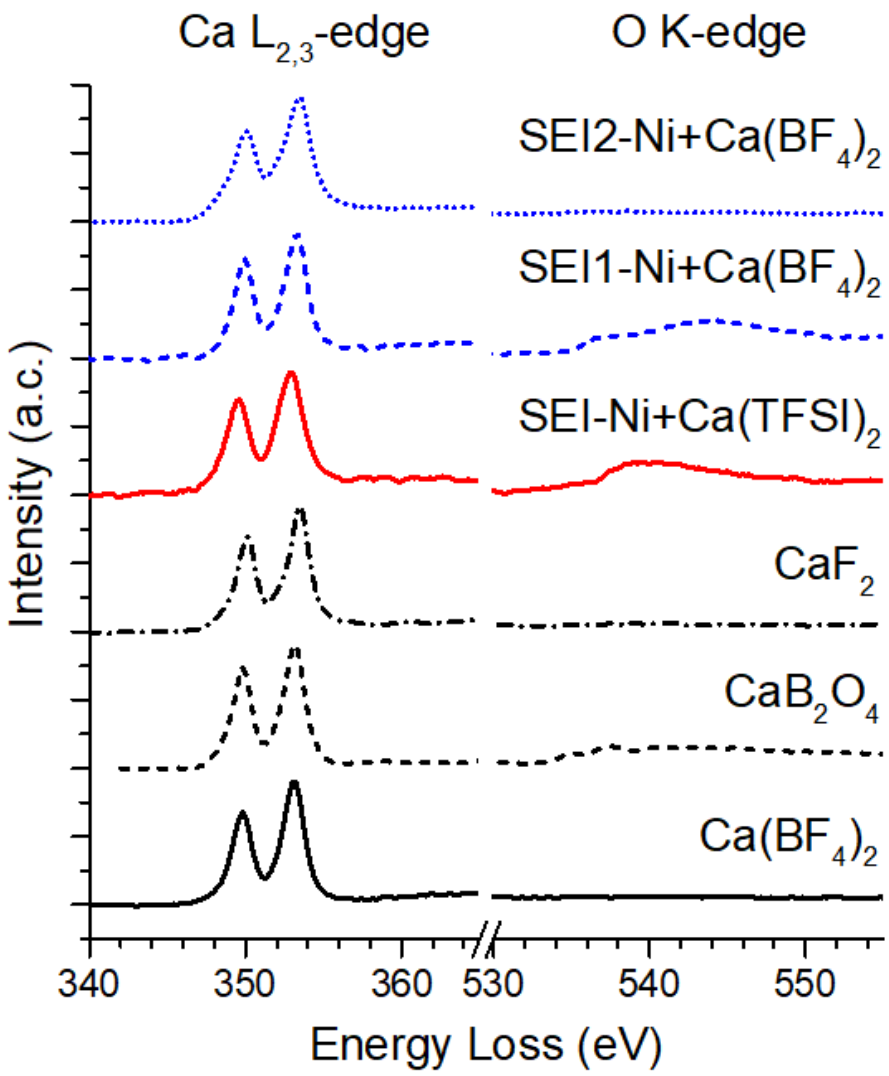

Figure S5. Normalized EELS spectra on the Ca L2,3-edge and O-Kedge for in the bottom and black the references ($Ca(BF_4)_2$, CaB_2O_4 and CaF_2) and in the top the SEI obtained with in red with $Ca(TFSI)_2$, in blue the "SEI1" and "SEI2" deposits (Figure 1c) in $Ca(BF_4)_2$ electrolyte.

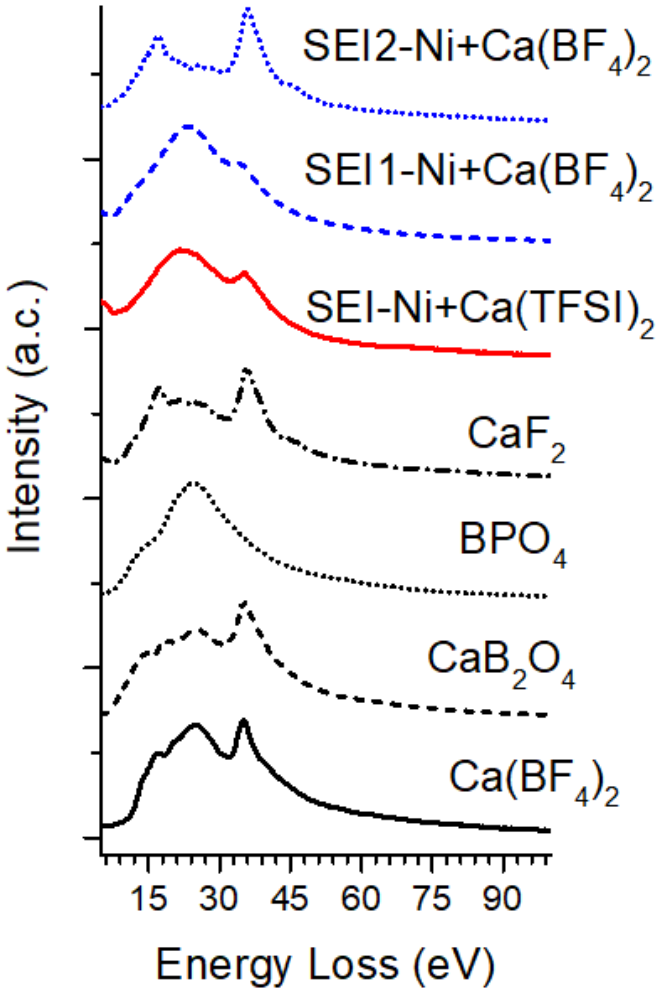

Figure S6. Normalized EELS spectra in the low loss area (plasmon contribution) for in the bottom and black the references ($Ca(BF_4)_2$, CaB_2O_4, CaF_2, and BPO_4) and in the top and blue the "SEI1" deposit (Figure 1c) in $Ca(BF_4)_2$ electrolyte. The peak observed at ~35,6 eV corresponds to Ca $M_{2,3}$-edge

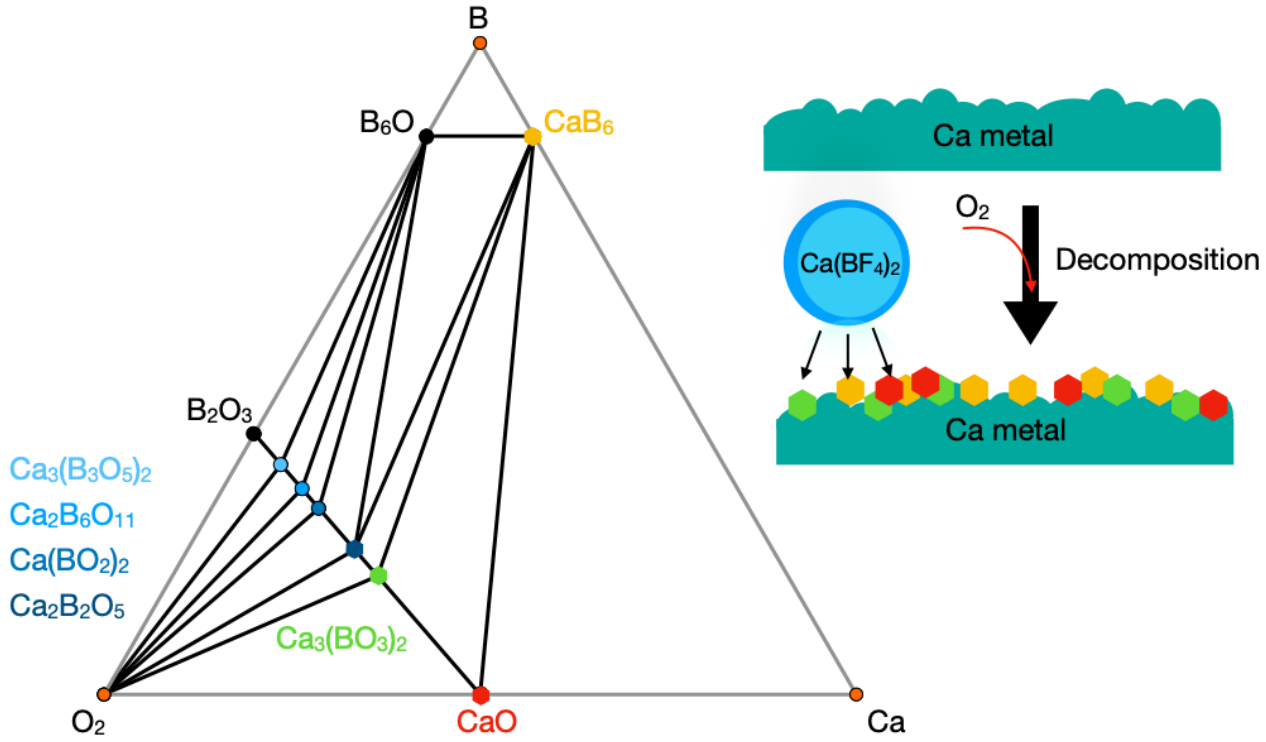

Figure S7. Left panel displays the computed ternary phase diagram for Ca-B-O system from first-principles calculations. The cartoon in the **right panel** shows a hypothetical mechanism of $Ca(BF_4)_2$ decomposition in the presence of O_2 and Ca metal mapped to the phase diagram on the **left panel**, red hexagon is CaO, yellow hexagon is CaB_6 and green hexagon $Ca_3(BO_3)_2$. Note CaF_2 is not shown explicitly in the right panel, but it is expected to form at the surface of Ca-metal as determined by the TEM micrographics. The phase diagram in the **left panel** shows that CaO and CaB_6 are the two compounds that should form spontaneously when B- and O-containing species are in contact with the Ca metal electrode.

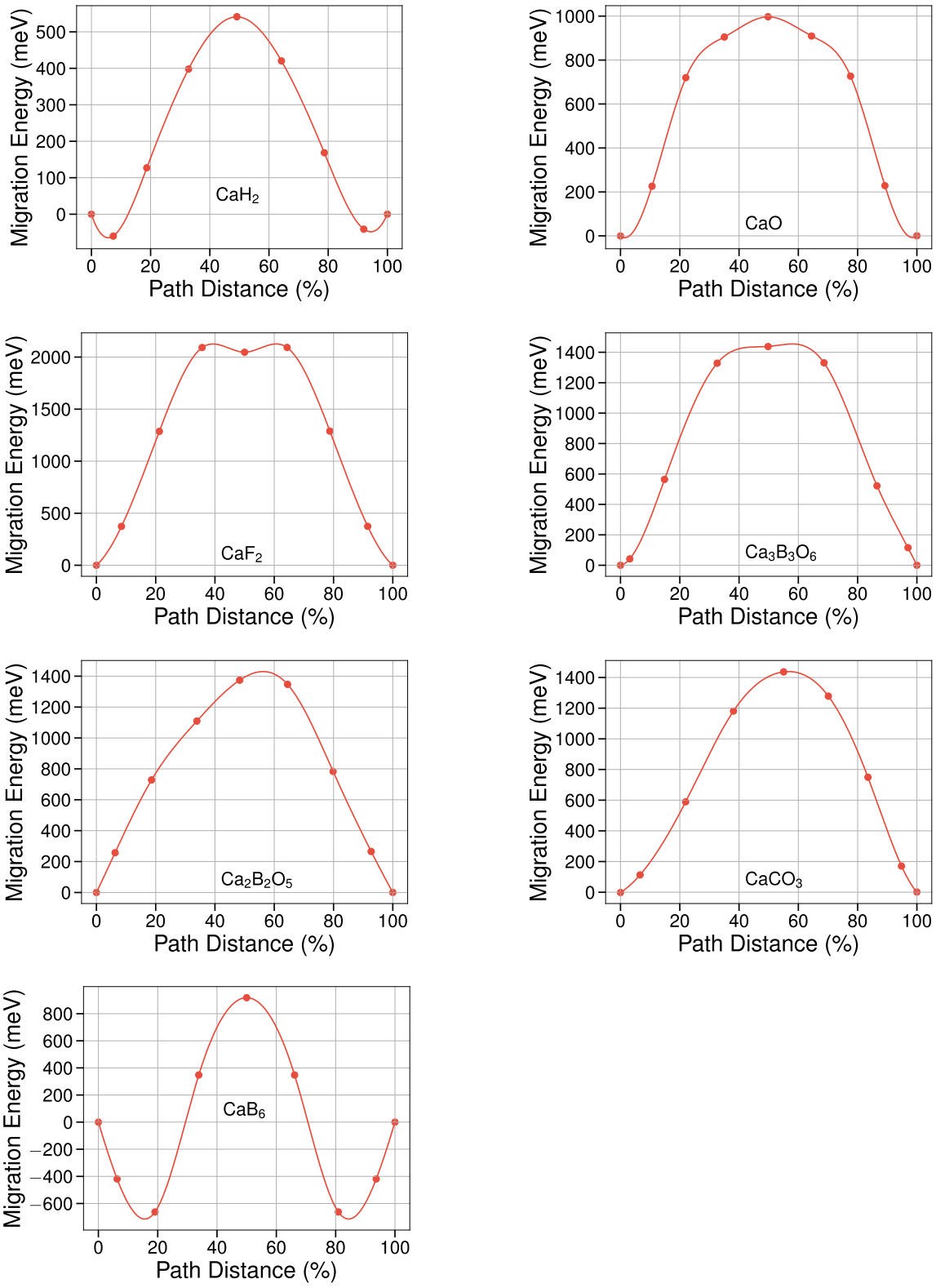

Figure S8. Computed migration energy paths for Ca^{2+} in a number of materials considered in this study.

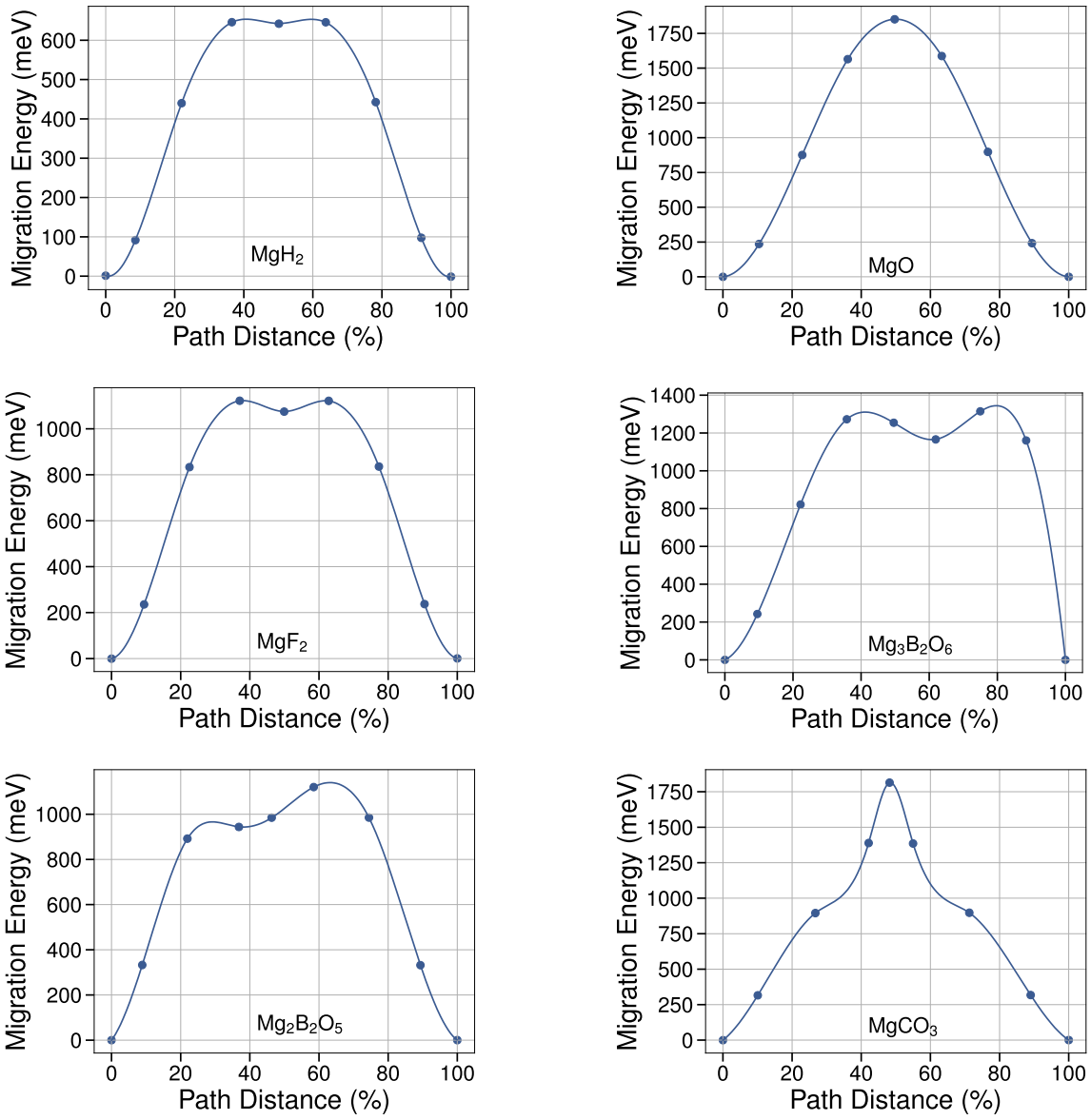

Figure S9. Computed migration energy paths for Mg^{2+} in a number of materials considered in this study.

4. REFERENCES

1 A. Ponrouch, C. Frontera, F. Bardé and M. R. Palacín, *Nat. Mater.*, 2016, **15**, 169–172.

2 L. Dupont, L. Laffont, S. Grugeon, S. Laruelle, V. Bodenez and J.-M. Tarascon, in *ECS Transactions*, ECS, 2007, vol. 3, pp. 139–153.

3 R. F. Egerton, *Electron Energy-Loss Spectroscopy in the Electron Microscope*, Springer US, New York, Second Edi., 1996.

4 D. Sheppard, R. Terrell and G. Henkelman, *J. Chem. Phys.*, 2008, **128**, 134106.

5 G. Henkelman, B. P. Uberuaga and H. Jónsson, *J. Chem. Phys.*, 2000, **113**, 9901–9904.

6 P. Hohenberg and W. Kohn, *Phys. Rev.*, 1964, **136**, B864–B871.

7 W. Kohn and L. J. Sham, *Phys. Rev.*, 1965, **140**, A1133–A1138.

8 J. P. Perdew, K. Burke and M. Ernzerhof, *Phys. Rev. Lett.*, 1996, **77**, 3865–3868.

9 G. Kresse and J. Furthmüller, *Phys. Rev. B*, 1996, **54**, 11169–11186.

10 S. Grimme, J. Antony, S. Ehrlich and H. Krieg, *J. Chem. Phys.*, 2010, **132**, 154104.

11 G. Kresse and D. Joubert, *Phys. Rev. B*, 1999, **59**, 1758–1775.

12 T. Chen, G. Sai Gautam and P. Canepa, *Chem. Mater.*, 2019, **31**, 8087–8099.

13 P. Canepa, G. Sai Gautam, D. C. Hannah, R. Malik, M. Liu, K. G. Gallagher, K. A. Persson and G. Ceder, *Chem. Rev.*, 2017, **117**, 4287–4341.